



ORIGINAL ARTICLE

Synthesis, spectroscopic characterisation, biological and DNA cleavage properties of complexes of nicotinamide



C. Surendra Dilip^{a,*}, V. Thangaraj^a, A. Paul Raj^b

^a Department of Chemistry, Anna University of Technology Tiruchirappalli, Tiruchirappalli 620 024, Tamil Nadu, India

^b Department of Chemistry, St. Joseph's College, Tiruchirappalli, Tamil Nadu, India

Received 14 March 2011; accepted 22 July 2011

Available online 31 July 2011

KEYWORDS

Nicotinamide;
Transition metal complexes;
Antimicrobial studies;
DNA binding

Abstract Transition metal complexes of nicotinamide with metal precursors such as Cr(III), Mn(II), Fe(III), Co(II), Ni(II), Cu(II) and Cd(II), were synthesized and characterised by physico-chemical and spectroscopic techniques. Based on analytical, spectral and magnetic moments, all the complexes are identified as distorted octahedral in structure. All the complexes are of the ML₁L₂ type. The shifts of the ν (C=N) (azomethine) and ν (C=O) (amide) stretches have been monitored in order to find out the donor sites of the ligands. Antibacterial and antifungal activities of the complexes were studied and the complexes were screened against bacteria and fungi. The activity data show that the metal complexes are more potent than the parent nicotinamide.

© 2011 Production and hosting by Elsevier B.V. on behalf of King Saud University. This is an open access article under the CC BY-NC-ND license (<http://creativecommons.org/licenses/by-nc-nd/3.0/>).

1. Introduction

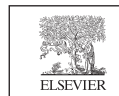
Heterocyclic compounds play a significant role in many biological systems, especially N-donor ligand systems being a component of several vitamins and drugs such as nicotinamide. Nicotinamide is known as a component of the vitamin B complex as well as a component of the coenzyme, nicotin-

amide adenine dinucleotide (NAD). These are more important for transfer of hydrogen in the cell breath. The presence of pyridine ring in numerous naturally abundant compounds, adducts of nicotinamide are also scientific interest. Therefore, the structure of nicotinamide has been the subject of many studies. Pyridine derivatives are associated with some important biological activities such as antitubercular, anthelmintic, fungicidal, antitumor and antibacterial activity (Cunha et al., 2005; Collen et al., 1997; Wolff, 1970; Gilman et al., 1980). Nicotinamide is found to be pharmacologically and physiologically active (Rosu et al., 2006; Filho et al., 1998; Turhan-Zitouni et al., 2001a,b; Deepa et al., 2005; Radhakrishnan et al., 1976). In this study, the preparation and structural elucidation of the transition metal complexes of nicotinamide were undertaken by using spectroscopic methods (UV, IR and EPR) and their biological activities such as antibacterial, antifungal and DNA cleavage which were also studied. Com-

* Corresponding author. Tel.: +91 9865605363.

E-mail addresses: cs_dilip@yahoo.co.in (C. Surendra Dilip), thangamraj@gmail.com (V. Thangaraj), apaul.raj63@gmail.com (A. Paul Raj).

Peer review under responsibility of King Saud University.



Production and hosting by Elsevier

parisons of the IR spectrum of nicotinamide with those of the metal complexes were useful in determining the atoms of the ligand that are coordinated with the metal ion. In addition, magnetic and electronic spectral measurements have been done in the case of coloured complexes. Electrochemical properties of the Cr(III)/Cr(II), Fe(III)/Fe(II) and Cu(II)/Cu(I) couple were studied extensively for understanding the factors that affect the donor environments.

2. Experimental

2.1. Materials and methods

All the chemicals used for the preparation of the ligands were of BDH quality, AR grade. Molar conductance of the complexes was measured using a Systronic conductivity bridge at room temperature in DMSO. Conductivity measurements ($\Omega^{-1} \text{ cm}^2 \text{ mol}^{-1}$) were carried out in DMF using a Tacussel conductivity bridge model. Magnetic susceptibilities were determined using a Guoy balance at room temperature (25 °C) with $\text{Hg}[\text{Co}(\text{SCN})_4]$ as standard. Perkin-Elmer PE 938 spectrophotometers were used to record the IR spectra using KBr pellets. UV-visible spectra were recorded in acetone and chloroform on a Perkin-Elmer model 550-S spectrometer. EPR spectra were recorded using Broker Ac 200 spectrophotometer. The electrochemical experiments were carried out using a Trace-Iab50 from radiometer which includes a polarographic analyser (Pol 150), a polarographic stand (MDE 150) and trace Master 5 software performed using a conventional three electrodes system. Potentials are expressed versus the Ag/AgCl (KCl mol l^{-1}) electrode separated from the test solution by a salt bridge containing the solvent/supporting electrolyte. A pre polished glassy carbon (GC) disc of 3 mm diameter (radiometer) was used as the working electrode and a platinum wire was the auxiliary electrode.

Solutions of CT DNA (calf-thymus DNA) in 50 mM NaCl/50 mM tris-HCl (pH = 7.2) gave a ratio of UV absorbance at 260 and 280 nm, A260/A280 of ~ 1.8 – 1.9 , indicating that DNA was sufficiently free of protein contamination. DNA concentration was determined by UV absorbance at 260 nm after 1:100 dilutions. The molar absorption coefficient was taken as $6600 \text{ M}^{-1} \text{ cm}^{-1}$. Stock solutions were kept at 4 °C and used within 4 days. Double distilled water was used to prepare the buffer.

2.2. Preparation of the complexes

Distilled ethanol (5.0 ml) and metal sulphates (0.50 m mol) are added to a 50 ml erlenmeyer flask fitted with a micro watch glass cover containing a magnetic stirring bar. Then the metal salt was dissolved in 1.0 mol of sodium sulphate and 2.0 m mol of nicotinamide. A large excess of ethanol is used, as it helps in the reaction completion. Heating and stirring the mixture was done for ~ 1 h. As the nicotinamide combines with the metal forms complexes, while cooling, the mixture crystals begin to form as a crust at the surface of the reaction mixture (Swamy and Pola, 2008; Swamy et al., 2003; Goeta et al., 2000).

2.3. General properties

Cr(III), Mn(II), Fe(III), Co(II), Ni(II) and Cu(II) complexes are coloured but the cadmium complexes are colourless (Table 1).

All the complexes are soluble in dimethyl formamide (DMF). Some of them are soluble only in nitrobenzene and acetone.

3. Results and discussion

The elemental analysis (Table 2) indicates that, all the metal complexes have 1:6 stoichiometry and are pale coloured amorphous substances, soluble in DMF. The molar conductance values obtained for these complexes at the concentration of 10^{-3} M are in the range of 10 – $20 \Omega^{-1} \text{ cm}^2 \text{ mol}^{-1}$. These values are too low to account for any dissociation of the complexes in DMF. Hence these complexes can be regarded as non-electrolytes. The ligand (L) is soluble in common organic solvents such as THF, $\text{C}_2\text{H}_5\text{OH}$, CH_2Cl_2 and DMSO. The octahedral metal complexes are highly soluble in DMSO and DMF and slightly soluble in CH_2Cl_2 and CHCl_3 .

3.1. Conductance

The observed molar conductance values of the complex in DMF are in the range of 10 – $20 \Omega^{-1} \text{ cm}^2 \text{ mol}^{-1}$ at room temperature. The value for 1:1 electrolyte in DMF is of the order of 65 – $90 \Omega^{-1} \text{ cm}^2 \text{ mol}^{-1}$. Hence from the conductivity measurement, it is concluded that the sulphate ions are covalently bonded to metal ions, which indicates that they act as ligands and not as simple ions. Based on the metal–ligand ratio calculated by the analytical data and the nature of the electrolytes given by the conductance measurements, compositions were assigned for the prepared complexes. From the magnetic and conductometric analysis it is predicted that the complexes may have the following structures $[\text{Cr}_2(\text{L}_2)_3(\text{L}_1)_9]$, $[\text{Mn}(\text{L}_2)(\text{L}_1)_5]$, $[\text{Fe}_2(\text{L}_2)_3(\text{L}_1)_9]$, $[\text{Co}_2(\text{L}_2)_3(\text{L}_1)_9]$, $[\text{Ni}(\text{L}_2)(\text{L}_1)_5]$, $[\text{Cu}(\text{L}_2)(\text{L}_1)_5]$ and $[\text{Cd}(\text{L}_2)(\text{L}_1)_5]$.

3.2. Magnetic moments

The Cr(III) complex showed a magnetic moment of 3.17 BM which is slightly lower than the spin only value of 3.87 BM expected for the three unpaired electrons, which offer possibility of an octahedral geometry. In this high spin complexes, the magnetic moments of the Fe(III) are close to the spin only value of 5.61 BM, because the ground state (derived, from the 5S state of the free iron) has no orbital angular momentum and there is no effective mechanism for introducing any by coupling with excited states. In the low spin complexes, with t_{2g}^5, e_g^0 configurations may have considerable orbital contributions to their moments at room temperature (Chandra et al., 2007). The experimental magnetic moments of the prepared Fe(III) complex indicates the high spin ($S = 5$) octahedral d^5 -system. The magnetic moment values for Cu(II), Co(II) and Ni(II) complexes are shown in Table 2. The magnetic moment of Co(II) complexes are in the range of 4.90 BM indicating that the Co(II) complexes are typically high spin complexes and having octahedral structure. The Ni(II) complexes exhibit the magnetic moment values in the range 3.8 BM, indicating octahedral co-ordination of the ligands around Ni(II) ion. The Cu(II) complexes exhibit magnetic moment in the range of 2.11 BM suggesting distorted octahedral nature for these complexes. It is obvious that the metal complexes possess anti-ferromagnetic properties by slight intramolecular antiferromagnetic spin exchange interaction for binuclear chromium

Table 1 Physical, analytical data of the complexes.

Complex	Empirical formula	Colour	Mol.	M.P.	Yield
			Wt	°C	%
[Cr ₂ (L ₂) ₃ (L ₁) ₉]	Cr ₂ C ₅₄ H ₅₄ N ₁₈ O ₂₁ S ₃	Pale brown	1468	270	70
[Mn(L ₂)(L ₁) ₅]	MnC ₃₀ H ₃₀ N ₁₀ O ₉ S	Mercedes red	758	295	70
[Fe ₂ (L ₂) ₃ (L ₁) ₉]	Fe ₂ C ₅₄ H ₅₄ N ₁₈ O ₂₁ S ₃	Reddish brown	1480	280	65
[Co (L ₂) (L ₁) ₅]	CoC ₃₀ H ₃₀ N ₁₀ O ₉ S	pink	760	275	68
[Ni(L ₂)(L ₁) ₅]	NiC ₃₀ H ₃₀ N ₁₀ O ₉ S	Green	762	272	60
[Cu(L ₂)(L ₁) ₅]	CuC ₃₀ H ₃₀ N ₁₀ O ₉ S	Pale blue	764	265	65
[Cd(L ₂)(L ₁) ₅]	CdC ₃₀ H ₃₀ N ₁₀ O ₉ S	Colourless	846	274	75

Table 2 Elemental analysis, magnetic moment, molar conductance of the complex.

Complex	% M	% C	% H	% N	% O	μ _{eff.} BM	Molar cond. (Ω ⁻¹ cm ² mol ⁻¹)
[Cr ₂ (L ₂) ₃ (L ₁) ₉]	7.05	67.21	4.15	14.01	7.60	3.17	18.25
	(7.45)	(67.32)	(4.55)	(14.00)	(7.05)		
	7.05	66.50	4.41	13.10	7.44	5.92	17.15
[Mn(L ₂)(L ₁) ₅]	(7.00)	(66.51)	(4.77)	(13.08)	(7.41)		
	7.56	64.84	3.42	13.17	7.54	5.61	17.38
[Fe ₂ (L ₂) ₃ (L ₁) ₉]	(7.51)	(64.86)	(3.79)	(13.15)	(7.53)		
	7.78	64.85	3.72	13.15	7.51	4.90	19.89
[Co (L ₂) (L ₁) ₅]	(7.74)	(64.88)	(3.79)	(13.16)	(7.53)		
	7.48	67.52	5.92	15.73	7.25	3.8	15.13
[Ni(L ₂)(L ₁) ₅]	(7.43)	(67.54)	(5.89)	(15.75)	(7.21)		
	8.02	53.41	3.56	16.35	6.49	2.11	18.26
[Cu(L ₂)(L ₁) ₅]	(7.96)	(61.56)	(3.52)	(16.32)	(7.47)		
	7.54	61.90	3.53	16.41	7.52	–	19.00
[Cd(L ₂)(L ₁) ₅]	(7.47)	(61.89)	(3.54)	(16.40)	(7.51)		

and iron, complexes with nicotinamide ligands. The absorption bands observed for the electronic spectra of the metal complexes also support the octahedral geometry (Turhan-Zito-uni et al., 2001a,b).

3.3. Infrared spectral analysis

The IR spectra of ligand (L) with its octahedral complexes have been studied in order to characterise their structures. The IR spectra of the free ligand and its metal complexes were carried out in the 4000–400 cm⁻¹ range. The IR spectra of all metal complexes were interpreted by comparing the spectra with those of the free ligand, and the results are listed in Table 3. The comparison of the band positions of various vibrations are ascertained with good evidence. In the infrared spectrum of the ligand, the band at 1385–1400 cm⁻¹ is due to asymmetric

C=N stretching vibration. The presence of δ(CONH₂) asymmetric stretching vibration is confirmed by the band at 1740 cm⁻¹ and the symmetrical stretching vibration is observed at 3350 cm⁻¹. In the infrared spectrum of metal sulphate complexes, the ν C=N stretching vibration were observed at 1560–1610 cm⁻¹ and was due to coordination of the nitrogen from C=N to the metal, stretching vibration for L reduced at the complex. The free nicotinamide ligand showed a strong peak at 1460 cm⁻¹ for L, which is characteristic of the imine ν (C=N) group. The ν (C=C) stretching vibrations are affected upon complexation and are situated at a frequency significantly different than the free ligands. Coordination of the nicotinamide ligands to the metal centre through the nitrogen atom is expected to reduce the electron density in the methine and imine link and hence lower the ν (C=C) and ν (C=N) absorption frequencies. The peak due to ν (C=C) is

Table 3 Characteristic IR bands (cm⁻¹) of the ligand and its complexes.

Ligand/complex	ν _{N-H} amide _{III}	ν _{C=O} amide _I	ν _{C=N} imine	ν _{C-N}	ν _{M-N}	ν _{M-SO4}
Nicotinamide	1532	1680	1612	1255		
[Cr ₂ (L ₂) ₃ (L ₁) ₉]	1537	1680	1560	1258	527	340
[Mn(L ₂)(L ₁) ₅]	1534	1682	1594	1262	523	342
[Fe ₂ (L ₂) ₃ (L ₁) ₉]	1535	1682	1583	1267	529	346
[Co ₂ (L ₂) ₃ (L ₁) ₉]	1533	1680	1610	1260	540	350
[Ni(L ₂)(L ₁) ₅]	1535	1684	1570	1272	535	342
[Cu(L ₂)(L ₁) ₅]	1532	1682	1597	1278	542	350
[Cd(L ₂)(L ₁) ₅]	1536	1685	1567	1285	555	355

slightly shifted to lower frequencies and appears between 1576 and 1579 cm^{-1} , indicating the coordination of the imine nitrogen to the metal.

Similarly the other metal complexes also show that the stretching frequency for the $\text{C}=\text{N}$ and $\text{C}=\text{C}$ are shifted to lower indicating that the metal is coordinated through the imine nitrogen atom. The peak at 1680 cm^{-1} corresponds to the asymmetric $\text{C}=\text{O}$ stretching vibration and the symmetric $\text{O}=\text{CN}$ stretching vibration observed at 1750 cm^{-1} confirms that all the complexes, the ligand do not coordinate with CONH_2 nitrogen.

The band at 1680 cm^{-1} which is assignable to nicotinamide *I* band arising mainly from the $\text{C}=\text{N}$ stretching vibration in free ligand is found to have no change in frequencies (1680–1685 cm^{-1}) in the metal complexes. The nicotinamide *III* band at 1532 cm^{-1} due to a coupled $\text{C}=\text{O}$ stretching mode move to higher wave numbers (1537–1532 cm^{-1}) compared to that of free ligands indicating the coordination of nicotinamide through the pyridine nitrogen. This results in the decreased $\text{C}=\text{N}$ bond order with concomitant increase in the $\text{C}-\text{O}$ bond order. The bands due to ν ($\text{C}-\text{N}-\text{C}$) and ν ($\text{C}-\text{O}-\text{C}$) remain almost unchanged in all the complexes indicating that the nitrogen and oxygen of carbonyl moiety are not involved in binding. The free ligand showed a medium intensity band at 3210 cm^{-1} assigned to ν NH vibrations, which has been observed in the 3203–3207 cm^{-1} region for the complexes. It can be observed that there is no considerable shift in the ν NH vibrations in the case of the complexes compared to the ligands indicating non-involvement of amide NH function in the coordination. A strong intensity band observed at 1675 cm^{-1} and a medium intensity band at 1630 cm^{-1} indicate that the ligands are assigned to ν ($\text{C}=\text{O}$) and ν ($\text{C}=\text{N}$) functions respectively. In the case of complexes the band due to ν $\text{C}=\text{O}$ was observed in the 1670–1676 cm^{-1} region, indicating its non-involvement in the complexation. The low frequency skeletal vibration due to $\text{M}-\text{N}$ stretching provides direct evidence of the complexation. In the present investigation, bands are observed in the 479–417 cm^{-1} region for ν $\text{M}-\text{N}$ vibrations, respectively (Chandra and Gupta, 2001; Rai et al., 2005). The occurrence of bands at \sim 1100 and \sim 600 cm^{-1} suggests the presence of free sulphate ion (Td) due to ν_3 and ν_4 mode of vibrations, respectively. However in complexes, an additional series of six bands appeared at \sim 1110, \sim 1040, \sim 970, \sim 645, \sim 600 and \sim 437 cm^{-1} indicating the coordination of sulphate group in monodentate manner through oxygen atom, the symmetry being lowered to C_3V upon coordination.

3.4. Electronic spectral analysis

Electronic spectra of ligand L and their metal complexes in DMF solutions have been recorded in the 200–1100 nm range.

The UV–Vis spectra of the ligand and metal complexes in DMF showed two to seven numbers of absorption bands between 268 and 734 nm (Table 4). The bands below 455 nm are mostly associated with intra ligand $\pi \rightarrow \pi^*$ and $n \rightarrow \pi^*$ transitions. In the electronic spectra of the ligand and their metal complexes, the presence of a wide range of bands is due to both $\pi \rightarrow \pi^*$, $n \rightarrow \pi^*$ and $d-d$ transitions and also due to charge transfer transition arising from π electron interactions between the metal and ligand that involves either a metal-to-ligand or ligand-to-metal electron transfer. The absorption bands observed within the range of 331–397 nm in DMF are mostly due to the transition of $n \rightarrow \pi^*$ of imine group corresponding to the ligand or metal complexes.

3.4.1. Manganese(II) complexes

The Mn(II) complex shows magnetic moment of 5.92 BM at room temperature corresponding to the five unpaired electrons. The electronic spectra of the Mn(II) complexes exhibit four weak intensity absorption bands in the range 17,794 ($\epsilon = 27 \text{ l mol}^{-1} \text{ cm}^{-1}$), 21,978 ($\epsilon = 35 \text{ l mol}^{-1} \text{ cm}^{-1}$), 25,974 ($\epsilon = 62 \text{ l mol}^{-1} \text{ cm}^{-1}$) and 35,425 cm^{-1} ($\epsilon = 129 \text{ l mol}^{-1} \text{ cm}^{-1}$), assigned to the transitions: ${}^6\text{A}_{1g} \rightarrow {}^4\text{T}_{1g}(4\text{G})$, ${}^6\text{A}_{1g} \rightarrow {}^4\text{E}_g$, ${}^4\text{A}_{1g}(4\text{G})$ (10B + 5C), ${}^6\text{A}_{1g} \rightarrow {}^4\text{E}_g(4\text{D})$ (17B + 5C) and ${}^6\text{A}_{1g} \rightarrow {}^4\text{T}_{1g}(4\text{P})$ (7B + 7C), respectively.

Electronic spectra of Mn(II) complexes, a strong band appearing at \sim 29400 cm^{-1} may be attributed to the $\pi-\pi^*$ transition of the $\text{C}=\text{N}$ group. The complexes in the visible region show very weak absorptions at \sim 21,700 and \sim 25,000 cm^{-1} , which may be assigned to ${}^6\text{A}_{1g} \rightarrow {}^4\text{E}_g(\text{G})$ and ${}^6\text{A}_1 \rightarrow {}^4\text{A}_1(\text{G})$ transitions of an octahedral (Hathaway and Billing, 1970). The β values of the complex lie at 0.871. β Value indicates the appreciable covalent character of the metal–ligand ' σ ' bond.

In Mn(II), the values *B* and *C* were calculated from the second and third transitions, because these transitions are free from the crystal field splitting. Slater Condon–shortly parameter F_2 and F_4 are related to the Racah parameter *B* and *C* are calculated as: $B = F_2 - 5F_4$ and $C = 35F_4$. On the basis of the above spectral studies distorted octahedral structures are suggested for the complexes.

3.4.2. Ferric complexes

The electronic spectra of the Fe(III) complex showed the strong bands at 17,932 and 13,122 cm^{-1} which are not possible to identify the type of the $d-d$ transition, due to a strong charge-transfer (CT) band tailing from the UV-region to the visible region. Magnetic moment of 5.61 BM was observed for the Fe(III) complex that is slightly lower than the magnetic moment of a high spin octahedral complex. Thus the structure of Fe(III) complex is tentatively interpreted to possess an octahedral geometry.

Table 4 Electronic spectral data and ligand field parameters of complexes.

Complex	ν_1	ν_2	ν_3	Dq	B'	β	$\beta\%$	ν_2/ν_1	ν_3/ν_2	' λ ' LFSE kcal mol $^{-1}$
$[\text{Cr}_2(\text{L}_2)_3(\text{L}_1)_9]$	12,345	18,654	24,378	1186	949	0.80	20.00	1.5	1.3	37.43
$[\text{Mn}(\text{L}_2)(\text{L}_1)_5]$	11,794	21,978	25,974	1124	980	0.871	13.90	1.8	1.2	34.86
$[\text{Fe}_2(\text{L}_2)_3(\text{L}_1)_9]$	13,122	17,932	–	1086	865	0.796	21.10	1.4	–	35.56
$[\text{Co}_2(\text{L}_2)_3(\text{L}_1)_9]$	8892	15,439	20,085	1002	749	0.778	23.03	1.7	2.1	27.17
$[\text{Ni}_2(\text{L}_2)(\text{L}_1)_5]$	13,810	15,151	25,316	1040	852	0.820	18.00	1.4	1.8	30.82
$[\text{Cu}(\text{L}_2)(\text{L}_1)_5]$	10,526	16,181	25,000	1020	875	0.857	14.30	1.5	1.6	33.36

3.4.3. Cobalt(II) complexes

The electronic spectrum of the cobalt complexes exhibited three bands at 15,674, 18,832 and 25,971 cm^{-1} that are assigned to the transitions ${}^4\text{T}_{1g}(\text{F}) \rightarrow {}^4\text{T}_{2g}(\text{F})$, ${}^4\text{T}_{1g}(\text{F}) \rightarrow {}^4\text{A}_{2g}(\text{F})$ and ${}^4\text{T}_{1g}(\text{F}) \rightarrow {}^4\text{T}_{1g}(\text{P})$, respectively, suggesting an octahedral geometry around the Co(II) ion. The magnetic moments of Co(II) complexes were found to be 4.90 BM also indicating octahedral geometry. Interelectronic repulsion parameter (B') of Co(II) complex shows 749 cm^{-1} which is less than the free ion (B) value of 971 cm^{-1} suggesting the considerable orbital overlap and delocalisation of electrons on the metal ion. The nephelauxetic ratio (β) for the Co(II) complex (0.778) is less than one, suggesting partial covalency in the metal ligand bond. The values Dq , $\beta\%$, LFSE and ν_2/ν_1 (Table 4) suggest the distorted octahedral geometry for Co(II) complex (Silverstein et al., 2007; Singh and Pheko, 2008).

3.4.4. Nickel(II) complexes

The absorption spectra of Ni(II) complexes display three $d-d$ transition bands at 12,108, 19,416 and 27,322 cm^{-1} which correspond to ${}^3\text{A}_{2g} \rightarrow {}^3\text{T}_{2g}$, ${}^3\text{A}_{2g} \rightarrow {}^3\text{T}_{1g}(\text{F})$ and ${}^3\text{A}_{2g} \rightarrow {}^3\text{T}_{1g}(\text{P})$. The magnetic moments of Ni(II) complexes were found to be 3.8 BM supporting the d^8 high spin distorted octahedral structure. The ligand field parameter such as Dq , B' , β , $\beta\%$ and LFSE have been calculated by using Band-fitting equation given by Underhill and Billing (Table 4). The ratio ν_2/ν_1 was found to be 1.4046 which is well within the range (1.40–1.61) and is indicative of octahedral stereochemistry for this Ni(II) complex (Kivelson and Neiman, 1961). The Racah parameter B' is 852 cm^{-1} , which is less than the free ion (B) value of 1040 cm^{-1} indicating the covalent character. The ratio ν_2/ν_1 and $\beta\%$ also support further the octahedral geometry around the Ni(II) ion (Wehrli et al., 1988). These observations reveal that the nickel complexes possess an octahedral geometry and D_3 symmetry.

3.4.5. Copper(II) complexes

The magnetic moment values of Cu(II) complexes are 2.11 BM that fall within the normal range observed for distorted octahedral complexes. From the results, Cu(II) complexes show, a single broad band in the range 18,920 cm^{-1} due to transition between ${}^2\text{E}_g \rightarrow {}^2\text{T}_{2g}$ suggesting tetragonal geometry. Tetragonal or square planar Cu(II) complexes are expected to give three bands. However, these three bands usually overlapped in tetragonal complexes, to give one broad absorption band. The electronic spectra and magnetic moment data for all Cu(II) complexes coupled with the analytical, conductance data suggest the tetragonal geometry for all the complexes.

3.4.6. Ligand field parameters

Various ligand field parameters were calculated and their values are listed in Table 4. The results show that the ligand field parameter values of the complexes were consistent with octahedral geometry. The ligand field strength, $10 Dq$, can be estimated roughly for each complex by the relationship of nonlinear for all the anisotropic ligands. The β values indicate the covalent character, which is due to the presence of σ and π bonds between the metal and ligands. Δ Values indicate the energy difference between the principle bands, which are formed due to ligand field absorption. This type of complex may have either C_{4v} or D_{4h} symmetry, which arises from the lifting of the degeneracy of the orbital triplet (in octahedral

symmetry) in the order of increasing energy or assuming D_{4h} symmetry. C_{4v} symmetry is ruled out because of the higher splitting of the first band. This suggests that it possesses distorted octahedral geometry around the metal ion.

3.5. EPR spectral analysis

3.5.1. EPR spectrum of Cu(II) complex

The EPR spectra of the Cu(II) complexes were recorded (Fig. 1) in a polycrystalline sample as well as in solution at room temperature in different frequencies. The g -values are calculated by using the expression,

$$G = 2.0023(1 - 4\lambda/10Dq),$$

where λ is the spin-orbit coupling constant for the metal ion.

The analysis of spectra gives the values for g_{\parallel} 2.22–2.27 and $g^{\perp} = 2.09 - 2.10$. The observed ' g ' values for the complexes are less than 2.3 in agreement with the covalent character of the metal ligand bond. The trend $g_{\parallel} > g^{\perp} > 2.0023$ observed for the complexes indicates that the unpaired electron is localised in dx^2-y^2 orbital of the Cu(II) ion and spectral features are characteristic of axial symmetry. Tetragonal elongated structure is confirmed for the aforesaid complex.

3.5.2. Chromium complex

The spin-orbit coupling constant from the free ion value 90 cm^{-1} of Cr(III) complex is reduced from its metal ion and this can be employed as a measure of metal-ligand covalency (Fig. 2). The values indicate that the complexes under study have a substantial covalent character. The g -values were calculated and found in the range of 1.97–1.99, corresponding to 6-coordinated geometry. It is possible to define a covalency parameter analogous to the nephelauxetic parameter, which is the ratio of the spin-orbit coupling constant for the complex and the free Cr(III) ions.

3.6. Thermal decomposition

The TG curves of the metal-nicotinamide complexes suggest that modes of decomposition resemble each other closely. All these complexes follow the same pattern of thermal decomposition. The complexes remain almost unaffected up to $\sim 70^\circ\text{C}$ (Table 5). After this, a slight depression is observed up to $\sim 110^\circ\text{C}$. The weight loss in this temperature range is equivalent to two water molecules in the complexes indicating them to be lattice water in conformity with our earlier observations from analytical and IR spectral investigations. The anhydrous

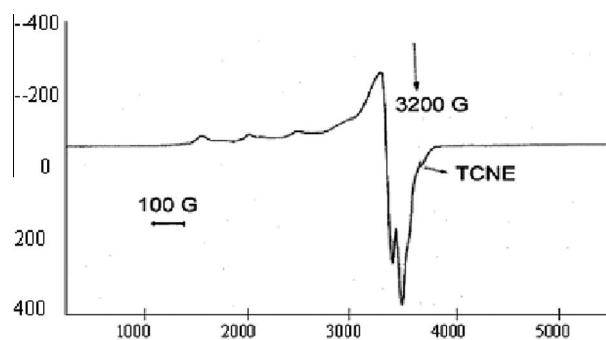


Figure 1 EPR spectrum of Cu(II) complex.

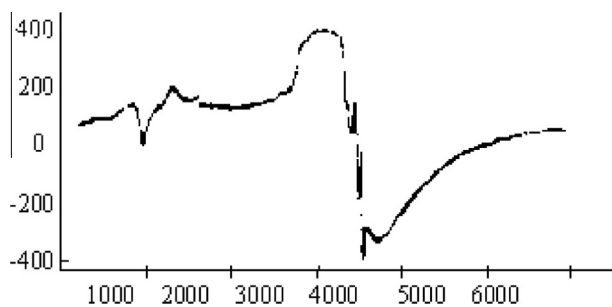


Figure 2 EPR spectrum of Cr(III) complex.

complexes remain stable up to ~ 300 °C and thereafter the complexes show rapid degradation presumably due to decomposition of organic constitution of the complexes as indicated by the steep fall in the percentage weight loss. The decomposition continues up to ~ 800 °C and reaches to a stable product in each complex as indicated by the constituency in weight in the plateau of the thermogram. The decomposition temperature varies for different complexes as shown in Table 5.

There is no mass loss observed up to 185 °C for the Cr complex. The sharp endothermic DTA peaks at 123–183 °C show that the complex melts before decomposition. The thermogravimetric curves of all the complexes show single stage decomposition wherein simultaneous decomposition and oxidation of the organic moiety and the volatilisation of chromium take place after 165–185 °C. There are broad endothermic peaks at 274 °C indicating slow decomposition of the complex. Due to the oxidation of the organic moiety two broad exothermic peaks appear between 290 °C and 355 °C for the complex. No such exothermic peaks were observed in the case of manganese complex. Due to volatilisation the weight of the final residue does not conform to any particular and product.

For Fe complex, there is no mass loss up to 181 °C, two endothermic peaks appeared at 80 and 120 °C, which are due to the decomposition and loss of coordinated water molecules. There afterwards, the complex shows single stage decomposition without giving any stable intermediate compound. A broad exothermic peak at 220 °C followed by an endothermic peak at 280 °C shows the oxidative process. The weight of the final residue almost corresponds to the formation of FeO.

3.7. Electro chemical studies

Cyclic voltammogram of cobalt complex recorded in 1.0 mM electrolyte containing DMSO is shown in Fig. 3a. The samples

were scanned in the range from -1.9 to $+1.9$ V at the scan rate of 20 mV S^{-1} . During the cathodic scanning process, Cobalt complexes show a reduction peaks at 0.7 V due to the deposition of Co(II) on electrode surface and an oxidation peak at 1.05 V due to the stripping of cobalt from the surface. Also a small reduction peak was observed about at -0.85 V, which is mainly attributed to the adsorption of the double hydroxide at the cathode. Under these conditions, the pH value near the cathode seems to rise due to the proton consumption. Therefore, the hydroxide of metal ion may be produced in the vicinity of the electrode.

The cyclic voltammogram of Cd(II) complex recorded from 0.1 M TBATFB in DMSO showed in Fig. 3b. Potential varied from -2.0 to 1.0 V at the scan rate of 50 mV s^{-1} . During the cathodic scan, no reducible species present from 1.0 to -0.85 V, cathodic peak observed at -1.2 V due to the dissolution of cadmium from the electrolyte solution. During the reverse process, three oxidation peaks were observed (-0.7 and -0.2 V and a peak at 0.45 V) which is corresponding to the oxidation of cadmium in three phases.

Cyclic voltammogram of chromium complex recorded in electrolyte containing water is shown in Fig. 4a. The samples were scanned in the range from -1.0 to $+1.0$ V at the scan rate of 20 mV S^{-1} . During the cathodic scanning process, chromium nicotinamide complex shows a reduction peaks at -0.25 V and an oxidation peaks at 0.8 V due to the stripping of chromium from the surface. Under these conditions, the pH value near the cathode seems to rise due to the proton consumption. Therefore, the hydroxide of metal ion may be produced in the vicinity of the electrode. Cyclic voltammogram of Ferric complex is recorded in 1 mM electrolyte containing water is shown in Fig. 4b. The samples were scanned in the range from -1.0 to $+1.0$ V at the scan rate of 20 mV S^{-1} . During the scanning process, a reduction peak was observed at 0.25 V due to the dissolution of hydroxide ion and the deposition of ferrous ion on the base metal. From the figure, we can conclude that the good electrochemical performance of the electrode can be attributed to its higher electrical conductivity and facile ionic transportation that are offered by the nicotinamide additive. This metal complex also undergoes transformation between +2 and +3, and the transformation between these two oxidation states is highly reversible.

3.8. Powder X-ray analysis

The XRD (Powder Pattern) of the complexes $[\text{Co}_2(\text{L}_2)_3(\text{L}_1)_9]$ and $[\text{Ni}_2(\text{L}_2)(\text{L}_1)_5]$ were indexed in X-ray diffractometer and the unit cell parameters have been calculated with the help

Table 5 Thermal analysis data of the complexes.

Complexes	Total wt. for TG (mg)	Temp. range of water loss	Water loss (%)	Temp. range of melting (°C)	Temp. range of decomposition (°C)
$[\text{Cr}_2(\text{L}_2)_3(\text{L}_1)_9]$	110	80–110	5.08	170–235	420–800
$[\text{Mn}(\text{L}_2)(\text{L}_1)_5]$	90	85–110	4.92	180–240	400–780
$[\text{Fe}_2(\text{L}_2)_3(\text{L}_1)_9]$	105	75–105	4.68	160–250	410–800
$[\text{Co}(\text{L}_2)(\text{L}_1)_5]$	90	78–105	4.46	150–220	385–750
$[\text{Ni}(\text{L}_2)(\text{L}_1)_5]$	110	80–105	6.23	155–230	370–750
$[\text{Cu}(\text{L}_2)(\text{L}_1)_5]$	105	75–110	6.02	160–245	350–760
$[\text{Cd}(\text{L}_2)(\text{L}_1)_5]$	95	72–105	5.43	190–260	430–750

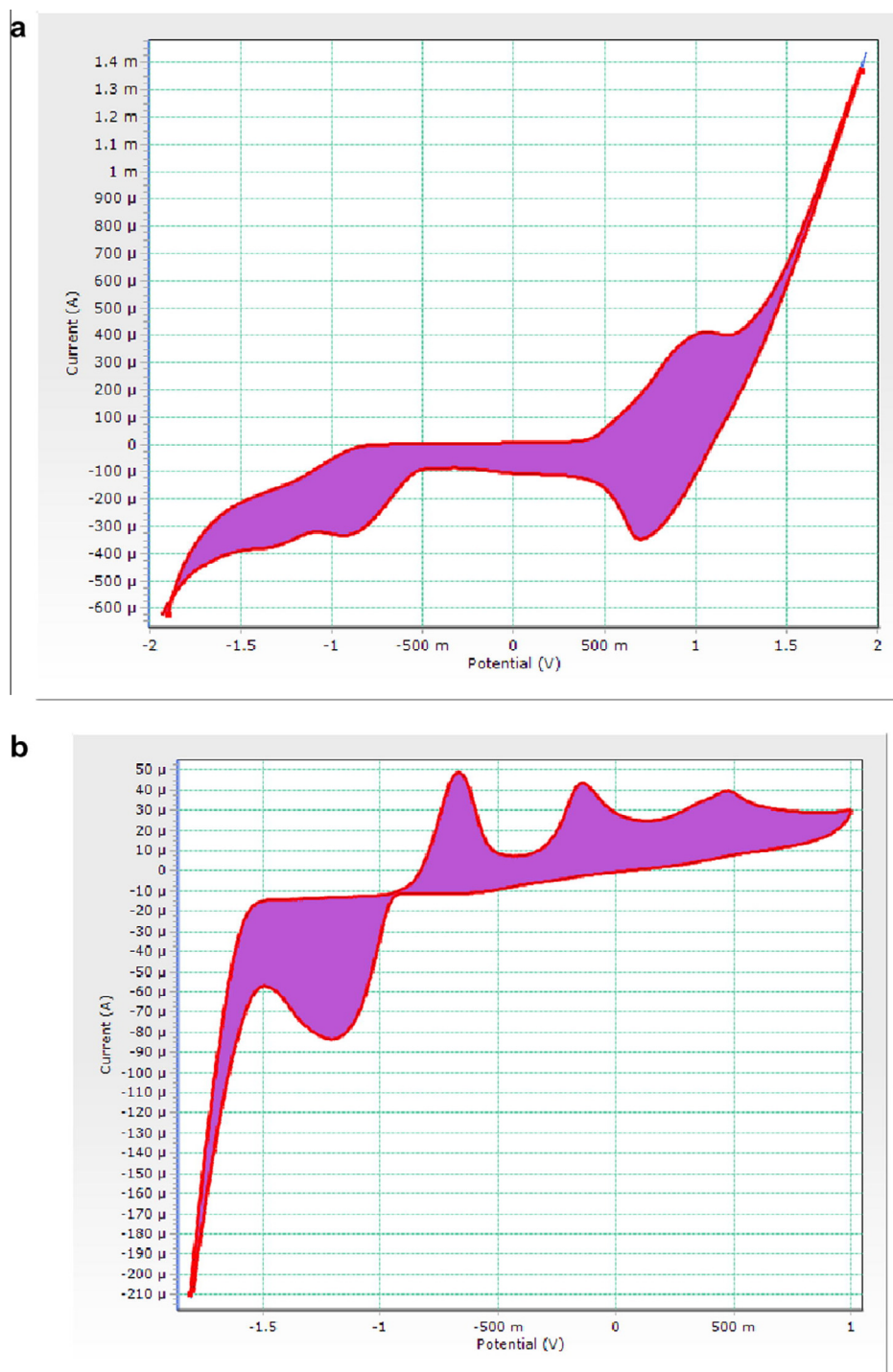


Figure 3 Cyclic voltammogram of (a) 1 mM Co(II) complex (b) Cd(II) complex in 0.1 M TBATFB in DMSO on Pt electrode, $V = 0.1 \text{ Vs}^{-1}$, (vs. $\text{Ag}|\text{Ag}^+$ electrode).

of a computer from 2θ values (Fig. 5). The direct constant parameters like A , B , C , α , β , γ and V (volume) are given in Table 6. The density of the complexes has been determined by the floatation technique in a saturated solution of NaCl, KBr and benzene separately.

The number of formula units per unit cell (n) was calculated from the relation

$$n = dNV/M,$$

where d = density of the compound, N = Avogadro's number, V = volume of the unit cell and M = molecular weight of the complex. The value of ' n ' is found to be 10 for both complexes which agree well with the suggested monoclinic structure of the complexes. In addition, we have carried out powder X-ray diffraction studies of complex. Powder XRD

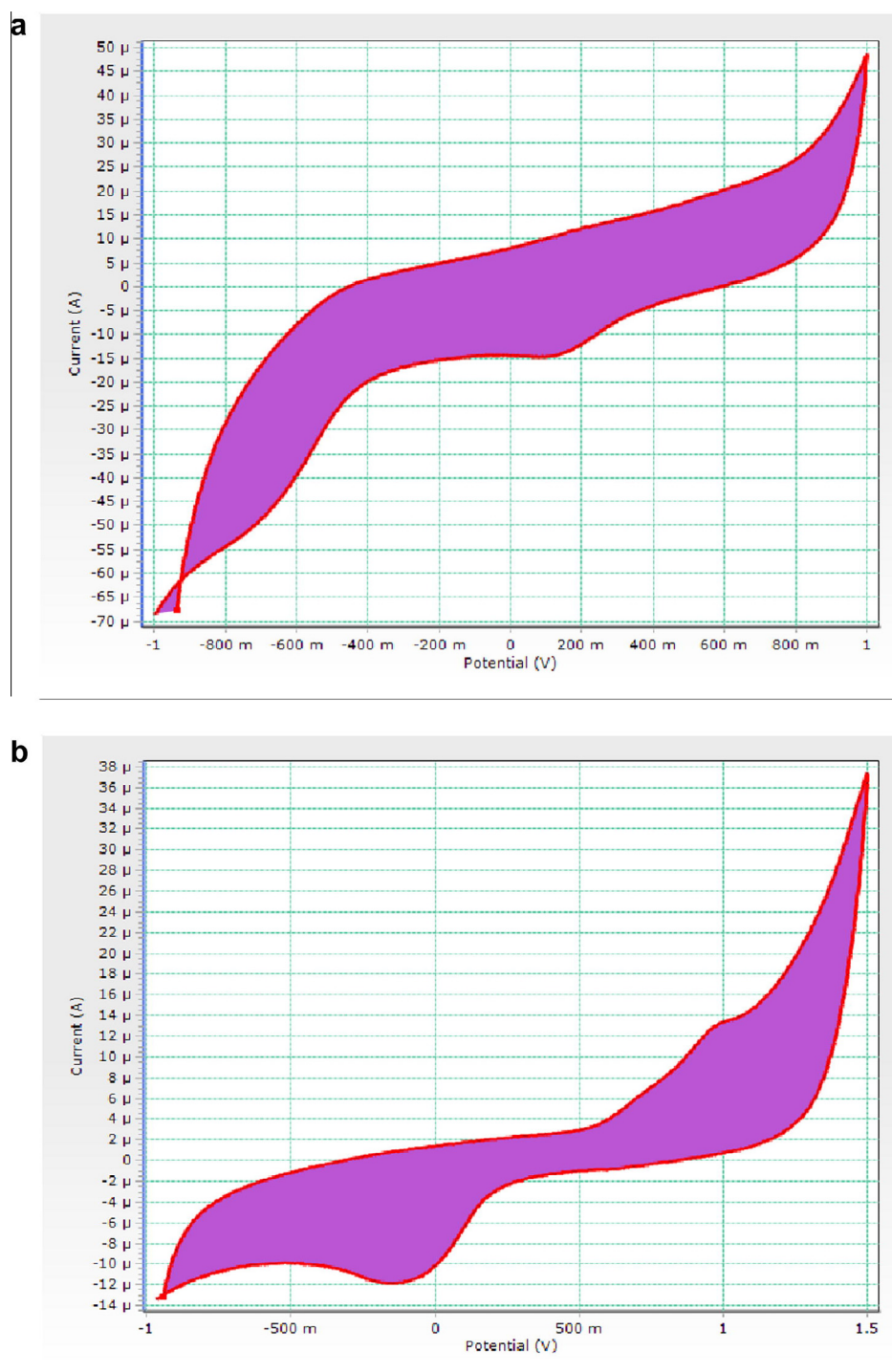


Figure 4 Cyclic voltammogram of (a) 1 mM Cr(III) complex (b) Fe(III) complex in 1 mM Fe(III) in DMSO on Pt electrode, $V = 0.1 \text{ Vs}^{-1}$, (vs. $\text{Ag}|\text{Ag}^+$ electrode).

pattern of $[\text{Co}(\text{L}_2)_3(\text{L}_1)_3]$ consists of 7 reflections in the range $5\text{--}50^\circ$ (2θ) the inter planar spacing (d) has been calculated from the positions of intense peaks using Bragg's relationship. The 2θ values with maximum intensity of the peak for ligand were found to be 5.709 (2θ) which correspond to $d = 15.4539$. All the important peaks have been indexed and the observed values of inter planar distance were compared with the calcu-

lated ones. It was found that there is good agreement between the calculated and observed values. The $(h^2 + k^2 + l^2)$ values are 1, 5, 27, 32, 58, 72 and 74. The presence of forbidden number confirms the tetragonal systems. This implies that the cobalt and nickel complexes are distorted octahedral in structure.

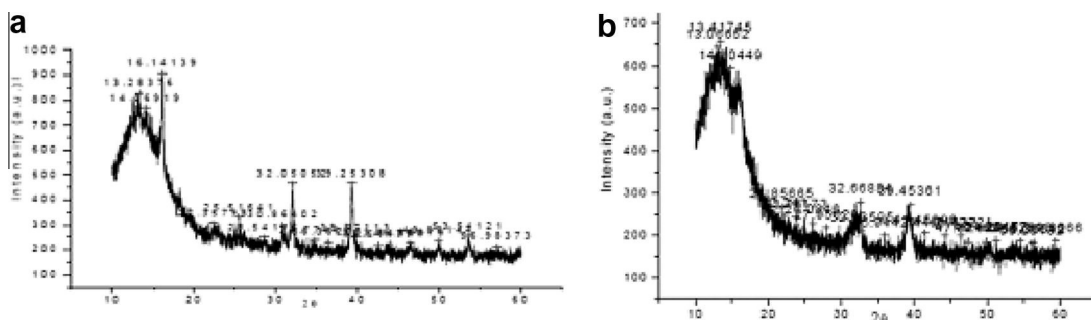


Figure 5 The XRD (powder pattern) of the complexes (a) $[\text{Co}_2(\text{L}_2)_3(\text{L}_1)_9]$ and (b) $[\text{Ni}_2(\text{L}_2)(\text{L}_1)_5]$.

3.9. Antimicrobial activity

The biological and medicinal potency of the coordination complexes has been established by their antitumor, antiviral and antimalarial activities. This characteristic property has been related to the ability of the metal ion to form complexes with ligand containing nitrogen donor atoms. The ligands and their complexes were screened for their antibacterial activity (Plakatouras et al., 1992) against *Escherichia coli* and *Staphylococcus aureus* and antifungal activity against (Assour, 1965) *Aspergillus niger* and *Aspergillus flavus* at the concentration of $100 \mu\text{g}/0.1 \text{ cm}^3$. The standard drugs streptomycin and clotrimazole were also tested for their antibacterial and antifungal activity at the same concentration under the conditions similar to that of the test compounds concentration.

3.10. Antibacterial activity

For *in vitro* antimicrobial activity, the investigated compounds were tested against the bacteria such as *Shigella dysenteriae*, *E. coli* and *Bacillus subtilis*. The minimum inhibitory concentration (MIC) values of the compounds against the growth of microorganisms are summarised in Table 7. It is observed that

the copper and cadmium complexes are more active in *Pseudomonas aeruginosa* and *B. subtilis*, respectively compared to other bacterial organisms. Nickel and cobalt complexes are moderately active in all bacterial organisms compared with standard streptomycin. From the results it is found that the copper complex is more active in *Streptococcus-β-haemolyticus* than the other complexes.

3.11. Antifungal activity studies

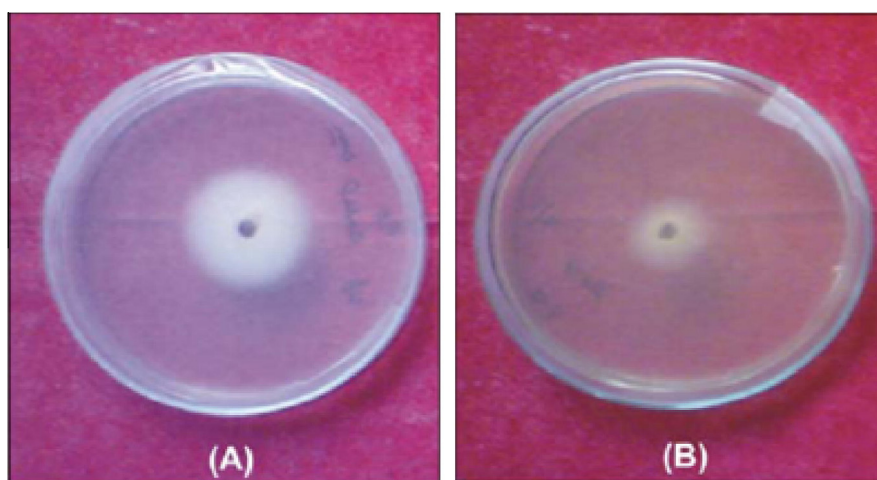
The results of the antifungal screening of the nicotinamide and the metal complexes with *Candida albicans*, *A. niger* and *Aspergillus fumigates* at concentration of $200 \mu\text{g}$ by disc method are given in the Fig. 6. Comparative studies of the ligands and their complexes indicated that metal complexes exhibit higher antifungal activity than the free ligands (Table 8). The antifungal activity results revealed that the ligands and their Cu(II), Co(II) and Ni(II), complexes have exhibited weak to good activity against *A. niger* and *A. flavus*. The ligand and its Cu(II) and Co(II) complexes show weak activity when compared to the standard drug clotrimazole. The order of the metal complexes follow $\text{Cu(II)} > \text{Cd(II)} > \text{Ni(II)} > \text{Co(III)} > \text{Mn(II)} > \text{Fe(III)} > \text{Cr(III)}$.

Table 6 X-ray powder pattern reports.

Compound	2θ Values			Unit cell parameters	Density (gcc)	n	Possible geometry
$[\text{Co}(\text{L}_2)_3(\text{L}_1)_9]$	13.284	13.936	16.141	$A = 13.300 \text{ \AA}$ $B = 20.543 \text{ \AA}$ $C = 6.985 \text{ \AA}$ $\alpha = 90.000^\circ$ $\beta = 102.325^\circ$ $\gamma = 90.000^\circ$ $V = 1864.37 \text{ \AA}^3$	0.83	1	Monoclinic
	17.228	18.130	18.264				
	19.300	21.756	22.659				
	25.010	25.516	30.914				
	32.051	39.253	41.659				
	42.244	43.849	46.389				
	47.308	48.194	49.881				
	50.032	51.419	53.174				
	53.541	53.976	54.076				
	54.277	55.680	56.148				
	56.265	56.466	56.766				
	56.833	56.984	57.184				
	57.836	58.087	58.621				
$[\text{Ni}(\text{L}_2)(\text{L}_1)_5]$	13.066	13.417	14.804	$A = 8.546 \text{ \AA}$ $B = 18.487 \text{ \AA}$ $C = 7.371 \text{ \AA}$ $\alpha = 90.000^\circ$ $\beta = 106.893^\circ$ $\gamma = 90.000^\circ$ $V = 1114.34 \text{ \AA}^3$	1.25	1	Monoclinic
	21.856	22.241	23.761				
	26.084	27.956	32.668				
	32.835	35.944	39.453				
	41.458	44.216	46.422				
	47.324	49.898	51.251				
	54.527	56.081	56.365				

Table 7 Antibacterial activities of the complexes and standard.

$\mu\text{g disc}^{-1}$	Diameter of zone of inhibition (in mm)														Ligand	
	C ₁		C ₂		C ₃		C ₄		C ₅		C ₆		C ₇		30	200
	30	200	30	200	30	200	30	200	30	200	30	200	30	200	30	200
<i>Gram positive bacteria</i>																
<i>Bacillus subtilis</i>	10	17	10	15	08	11	13	20	11	17	14	19	15	21	07	09
<i>Streptococcus-β-haemolyticus</i>	11	16	13	16	11	15	12	17	12	17	16	21	12	16	08	11
<i>Gram negative bacteria</i>																
<i>Shigella dysenteriae</i>	12	18	12	17	12	12	15	10	13	15	12	14	11	18	06	08
<i>Pseudomonas aeruginosa</i>	14	22	14	15	14	14	16	11	14	16	11	17	13	16	09	11
<i>Escherichia coli</i>	13	21	13	16	13	16	14	12	11	09	10	16	12	16	08	10

**Figure 6** Anti fungal activity of *Aspergillus flavus* of (A) ligand (B) $[\text{Ni}(\text{L}_2)(\text{L}_1)_5]$.**Table 8** Antifungal activities of the complexes and standard.

$\mu\text{g disc}^{-1}$	Diameter of zone of inhibition (in mm)								Ligand
	C ₁	C ₂	C ₃	C ₄	C ₅	C ₆	C ₇	200	
<i>Candida albicans</i>	15	10	17	15	19	22	17	11	
<i>Aspergillus niger</i>	17	10	18	15	18	23	19	10	
<i>Aspergillus fumigates</i>	18	11	15	13	20	21	18	13	

The higher activity of metal complexes can be explained on the basis of overtones concept and chelation theory. According to overtones concept of cell permeability, the lipid membranes that surround the cell favour the passage of only the lipid soluble material due to which lip solubility is an important factor, which controls antimicrobial activity. On chelation, the polarity of metal ion will be reduced to a greater extent due to the overlap of the ligand orbital and partial sharing of the positive charge of the metal ion with donor group. Further it increases the delocalisation of pi-electron over the whole chelate ring, lyophilizes, enhances the penetration of the complexes into lipid membranes blocking the metal binding sites in the enzymes of microorganisms. These complexes also disturb the respiration process of the cell and thus block the synthesis of protein that restricts further growth of the organism.

3.12. DNA cleavage studies

The metal complexes were able to convert super coiled DNA into open circular DNA. The general oxidative mechanisms proposed account for DNA cleavage by hydroxyl radicals. The general oxidative mechanisms proposed account for the abstraction of a hydrogen atom from sugar units predicting the release of specific residues arising from transformed sugars, depending on the position from which the hydrogen atom is removed. The cleavage is inhibited by the free radical scavengers implying that hydroxyl radical or peroxy derivatives mediate the cleavage reaction. The reaction is modulated by a metallo complex bound hydroxyl radical or a peroxy species generated from the co-reactant H_2O_2 .

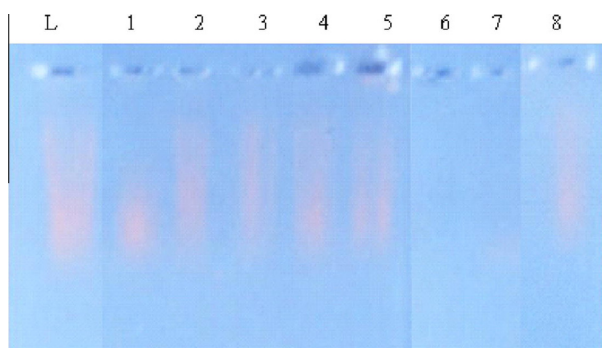


Figure 7 DNA cleavage studies of ligand and metal complexes.

In the present study, the CT-DNA gel electrophoresis experiment was conducted at 35 °C using our synthesized complexes in the presence of H_2O_2 as an oxidant. It was found that, at very low concentrations, few complexes exhibit nuclease activity in the presence of H_2O_2 . Control experiment using DNA alone does not show any significant cleavage of CT-DNA even on longer exposure time. Hence, we conclude that the copper complex cleaves DNA as compared with control DNA, while other complexes do not cleave DNA in the presence of H_2O_2 . Probably this may be due to the formation of redox couple of the metal ions and its behaviour.

The redox property of the metal complexes mediates oxidation of nucleic acids. In oxidative DNA cleavage mechanism, metal ions in the complexes react with H_2O_2 to generate the hydroxyl radical which attacks at the C4' position of the sugar moiety and finally cleaves the DNA. Copper complex reacts with H_2O_2 to produce hydroxyl radical, hydroxyl ion and Cu(II) form. The formation of hydroxyl radical by the copper complex is further compared with other complexes with H_2O_2 . Hence, copper complex can promote redox mediated cleavage of DNA reaction on sugar ring. The Cu(II) ion formation is supported by electrochemical study. Further, the presence of a smear in the gel diagram indicates the presence of radical cleavage.

As can be seen from the results (Fig. 7), at a very low concentration, few complexes exhibit nuclease activity in the presence of H_2O_2 . Control experiment using DNA alone (lane 1) does not show any significant cleavage of CT-DNA even on longer exposure time. From the observed results, we conclude that the complexes, copper complex (lane 6), nickel complex (lane 7) and cobalt complex (lane 8) cleave DNA as compared to control DNA while other complexes (lanes 1–5) do not cleave DNA in the presence of H_2O_2 . Probably this may be due to the formation of redox couple of the metal ions and its behaviour. Further, the presence of a smear in the gel diagram indicates the presence of radical cleavage.

4. Conclusion

Based on analytical, conductance, magnetic, infrared, electronic spectral data, EPR, CV, TGA and X-ray powder pattern, all these complexes are assigned to be in octahedral geometry and exhibit coordination number six. Biological studies of these complexes reveal that these complexes show better activity compared to their respective ligands. It is further confirmed on the basis of considerable low value of

magnetic moments in the case of Cu(II), Ni(II) and Co(II) complexes, which indicate antiferromagnetic coupling interaction between the two metal centres in the complexes. The value covalency factor (β) and orbital reduction factor (k) suggest the covalent nature of the complexes. The electrochemical properties of the metal complexes revealed the quasi-reversible one electron/two electron transfer redox process. The nicotinamide and some of the metal complexes were found to be active against some of the representative bacterial and fungal strains.

The screening of biological activities of ligand and its complexes against the fungi *Alternaria brassicae*, *A. niger* and *Fusarium oxysporum* and the pathogenic bacteria *Xanthomonas campestris* and *P. aeruginosa* indicates that the complexes show the enhanced activity in comparison to free ligand. The complexes, copper nickel and cobalt complexes cleave DNA as compared to control DNA while other complexes do not cleave DNA in the presence of H_2O_2 .

References

- Assour, J.M., 1965. Electron spin resonance of tetraphenylporphine chelates. *J. Chem. Phys.* 43, 2477–2489.
- Chandra, S., Gupta, K., 2001. Synthesis and spectral studies on chromium (III), manganese (II), iron (III), cobalt (II), nickel (II) and copper (II) complexes of fourteen membered and sixteen membered macrocyclic ligand. *Indian J. Chem.* 40A, 775–779.
- Chandra, S., Gupta, L.K., Agrawal, S., 2007. Modern spectroscopic and biological approach in the characterization of a novel 14-membered [N4] macrocyclic ligand and its transition metal complexes. *Trans. Met. Chem.* 32, 240–245.
- Collen, S.A.J., Everaerts, F.M., Huf, F.A., 1997. Characterization of ^{60}Co γ -radiation induced radical products of antipyrine by means of high-performance liquid chromatography, mass spectrometry, capillary zone electrophoresis, micellar electrokinetic capillary chromatography and nuclear magnetic resonance spectrometry. *J. Chromatogr. Acta* 755, 95–103.
- Cunha, S., Oliveira, S.M., Rodrigues Jr, M.T., Bastos, R.M., Ferrari, J., de Oliveira, C.M.A., Kato, L., Napolitano, H.B., Vencato, I., Lariucci, C., 2005. Structural studies of 4-aminoantipyrine derivatives. *J. Mol. Struct.*, 32–39, 752.
- Deepa, K., Madhu, N.T., Radhakrishnan, P.K., 2005. Cadmium(II) complexes of 1,2-di(imino-4'-antipyrinyl)ethane. *Synth. React. Inorg. Met.-Org. Nano-Met. Chem.* 35, 883–888.
- Filho, V.C., Correa, R., Vez, Z., Calixto, J.B., Nunes, R.J., Pinheiro, T.R., Andricopulo, A.D., Yunes, R.A., 1998. Further studies on analgesic activity of cyclic imides. *Farmaco* 53, 55–57.
- Gilman, A.G., Goodman, L.S., Gilman, A., 1980. The pharmacological basis of therapeutics. Macmillan Publishing Co, New York, USA.
- Goeta, A.E., Howard, J.A.K., Maffeo, D., Puschmann, H., Williams, J.A.G., Yufit, D.S., 2000. Copper(II) complexes of the isomeric tetraazamacrocyclic ligands 1, 11- and 1, 8-bis-(2-pyridylmethyl)-1, 4, 8, 11-tetraazacyclotetradecane and of the 1, 4, 8, 11-tetraazacyclotetradecane-5–12-dione analogue at neutral and basic pH. *J. Chem. Soc. Dalton Trans.*, 1873–1880.
- Hathaway, B.J., Billing, D.E., 1970. The electronic properties and stereochemistry of mono-nuclear complexes of the Copper(II) ion. *Coord. Chem. Rev.* 5, 143–207.
- Kivelson, D., Neiman, R., 1961. ESR studies on the bonding in copper complexes. *J. Chem. Phys.* 35, 149–155.
- Plakatouras, J.C., Perlepes, S.P., Mentzafos, D., Terzis, A., Bakas, T., Papaefthymiou, V., 1992. Coordination chemistry of corrosion inhibitors of the benzotriazole type: Preparation and characterization of Cobalt(II) complexes with 1-Methylbenzotriazole (Mehta)

- and the crystal structures of $[\text{CoCl}_2(\text{Mebta})_4]$, $\text{Trans-}[\text{Co}(\text{NCS})_2(\text{Mebta})_4]$, $\text{Trans-}[\text{Co}(\text{NCS})_2(\text{MeOH})_2(\text{Mebta})_2]$ and $\text{Cis-}[\text{Co}(\text{NO}_3)_2(\text{Mebta})_2]$. *Polyhedron* 11, 2657–2672.
- Radhakrishnan, T., Joseph, P.T., Prabhakaran, C.P., 1976. Copper(II) complexes of salicylal-4-amino antipyrine and 2-hydroxy naphthal-4-amino antipyrine. *J. Inorg. Nucl. Chem.* 35, 2211–2220.
- Rai, A., Sengupta, S.K., Pandey, O.P., 2005. Lanthanum(III) and praseodymium(III) complexes with isatin thiosemicarbazones. *Spectrochim. Acta A* 61, 2761–2765.
- Rosu, T., Pasculescu, S., Lazar, V., Chifiriuc, C., Cernat, R., 2006. Copper(II) complexes with ligands derived from 4-amino-2, 3-dimethyl-1-phenyl-3-pyrazoline-5-one. *Molecules* 11, 904914.
- Singh, G.S., Pheko, T., 2008. Spectroscopic Characterization of the 1-Substituted 3,3'-Diphenyl-4-(2'-hydroxyphenyl)azetidine-2-ones: Application of ^{13}C NMR, $^1\text{H-}^{13}\text{C}$ COSY NMR and Mass Spectroscopy. *Spectrochim. Acta. Part A* 70, 595–600.
- Silverstein, K.A., Moskal, W.A.J., Wu, H.C., Underwood, B.A., Graham, M.A., Town, C.D., VandenBosch, K.A., 2007. Small cysteine-rich peptides resembling antimicrobial peptides have been under-predicted in plants. *Plant J.* 51, 262–280.
- Swamy, S.J., Pola, S., 2008. Spectroscopic Studies on Co(II), Ni(II) Cu(II) and Zn(II) complexes with a N_4 -macrocyclic ligands. *Spectrochim. Acta A* 70, 929–933.
- Swamy, S.J., Veerapratap, B., Nagaraju, D., Suresh, K., Someshwar, P., 2003. Non-template synthesis of ' N_4 ' di- and tetra-amide macrocyclic ligands with variable ring sizes. *Tetrahedron* 59, 10093–10096.
- Turhan-Zitouni, G., Sivaci, M., Kilic, F.S., Erol, K., 2001a. Synthesis of some triazolyl-antipyrine derivatives and investigation of analgesic activity. *Eur. J. Med. Chem.* 36, 685–689.
- Turhan-Zitouni, G., Sivaci, M., Kilic, F.S., Erol, K., 2001b. Synthesis of some tiazolyl-antipyrine derivatives and investigation of analgesic activity. *Eur. J. Med. Chem.* 36, 685–689.
- Wehrli, F., Shaw, D., Kneeland, J.B., 1988. *Biological Magnetic Resonance Imaging: Principles, Methodology, Applications*. VCH, New York.
- Wolff, M.E. 1970. *Burger's Medicinal Chemistry*, third ed., vol. 1. Wiley, New York, USA.